Peer-reviewed version available at *Materials* **2020**, *13*, 3739; doi:10.3390/ma13173739

Article

Hot Deformation Behavior of Cu-Sn-La Polycrystalline Alloy Prepared by Upcasting

Siming Hua[1, 2], Pingze Zhang[1], Zili Liu[1], Lin Yang[2]

[1] College of Materials Science and Technology, Nanjing University of Aeronautics and Astronautics, Nanjing, 210000, China ; huasiming1987@126.com

[2] China Railway Construction Electrification Bureau Group Kangyuan New Material Co. ,Ltd, Jinjiang 214500,China ; huasiming1987@126.com

* Correspondence: zhangpingze@nuaa.edu.cn; Tel.: +86-13951883686

Abstract: In this study, the hot deformation of Cu-0.55Sn-0.08La (wt.%) alloy was studied using gleeble-3180 testing machine at deformation temperatures of 400–700 °C and various strain rates. The stress–strain curve showed that the hot deformation behavior of Cu-0.55Sn-0.08La (wt.%) alloy was significantly affected by work hardening, dynamic recovery, and dynamic recrystallization. The activation energy Q was calculated as 261.649 kJ mol^{-1} and hot compression constitutive equation was determined as $\dot{\varepsilon} = [\sinh(0.00651\sigma)]^{10.2378} \cdot \exp\left(33.6656 - \frac{261.649}{RT}\right)$. The microstructural evolution of the alloy during deformation at 400 °C revealed the presence of both slip and shear bands in the grains. At 700 °C, dynamic recrystallization grains were observed but recrystallization was incomplete. In summary, these results provide the theoretical basis for continuous extrusion process of alloys with promising application prospects in the future.

Keywords: Cu-Sn-La alloy; stress–strain; hot deformation; constitutive equations; dynamic recrystallization

1. Introduction

Copper alloys are structural and functional materials with excellent electrical and mechanical properties. These features make them suitable for applications in designing frame of large-scale integrated circuits, contact wires of electrified railway [1], lining of molds, and conductors for high pulse magnetic fields and traction motor rotors [2], among others.

Many studies have so far been published on the thermal deformation behavior of copper alloys, including Cu-Fe alloy [3,4], Cu-Ni-Si alloy [5,6], Cu-Ag alloy [7] and Cu-Al_2O_3 composites [8], Cu-Cr-Zr alloy [9,10], Cu-Cr-Zr-Ce, Nd, Y alloy [11–13], Cu-Mg alloy [14,15], and Cu-Al alloy [16–17]. However, only a few studies have been published on Cu-Sn alloys used in contact wires of electrified railways. On the other hand, continuous extrusion process is advantageous in terms of low energy consumption and high yield, thereby widely used in the production of contact wires for electrified railways. However, contact wires based on copper alloys still suffer from limitations such as high deformation temperatures, large deformation resistances, and complex thermal deformation behaviors. As a result, the optimization process of continuous extrusion remains extremely complex, and studies dealing with hot deformation behavior of Cu-0.55Sn alloy should help optimize the deformation behavior of Cu-Sn alloys via continuous extrusion process. Furthermore, the addition of small amounts of rare earth elements into copper alloys could purify the matrix and grain boundary, improve the conductivity, as well as improvingthe soften temperature and strength of the alloy [18]. For instance, the performance of Cu-0.55Sn alloys could be improved by adding 0.08%La.

In this study, the hot deformation behavior of Cu-0.55Sn-0.08La alloy was studied in an effort to provide the theoretical basis for optimizing the continuous extrusion process. The results indicated that the hot deformation behavior of Cu-0.55Sn-0.08La (wt.%) alloy was significantly affected by work hardening, dynamic recovery, and dynamic recrystallization. The activation energy Q and

Peer-reviewed version available at Materials 2020, 13, 3739; doi:10.3390/ma13173739

constitutive equation of hot deformation were determined by examining the relationships among hot compression flow stress and strain, strain rate, and deformation temperature of Cu-0.55Sn-0.08La alloy.

2. Materials and Methods

First, electrolytic copper (purity 99.99%), Sn (purity 99.95%), and pure block La (purity 99.5%) were together melted in a power frequency induction furnace. The molten copper liquid was then continuously cast into a Cu-Sn-La alloy rod billet (diameter 20 mm) using up-casting machine for further use. The mass fractions of alloy elements were determined as 0.55%Sn, 0.08%La, and Cu balance. Next, the continuous casting rod (diameter 20 mm) was cut by Lathe and Wire Electrical Discharge Machining (WEDM) into samples with size of Φ8 mm × 12 mm.

Table 1. Specification of properties of Cu-Sn-La alloy

	tensile strength/MPa	rockwell hardness/HRA	elongation/%
Cu-0.55Sn-0.08La	223.9	80.2	45.4

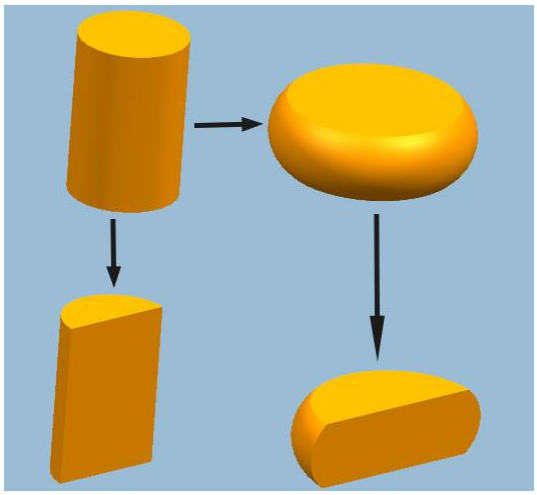

Figure 1. Schematic illustration of hot compression and metallographic samples.

The isothermal compression tests were conducted using a Gleeble-3180 simulator at deformation temperatures ranging from 400 to 700 °C (400, 500, 600, and 700 °C) and strain rates from 0.01 to 10 s^{-1} (0.01, 0.05, 0.1, 1, and 10 s^{-1}). Under each condition, compression tests were carried out once. All specimens were heated at heating rate of 5 K s^{-1} and kept for 180 s at the deformation temperature before isothermal compression. The specimens were then deformed to height reductions of 60%. Before testing, the two ends of each specimen were lubricated to prevent uneven deformation during hot compression deformation. After compression testing, the specimens were immediately quenched in water to maintain the state of the deformed tissue. The un-deformed and deformed specimens were then sectioned parallel to the compression axis (Figure 1). The specimens were mechanical polished and then etched in a solution containing $FeCl_3$ (3 g), HCl (2 mL), and C_2H_6O (96 mL). The microstructures were examined by optical microscopy (OM, LEICA DM2500M).

3. Results and discussion

3.1. Stress–strain behaviors of Cu–0.55Sn–0.08La alloy

The stress–strain behaviors of Cu–0.55Sn–0.08La alloy at various strain rates and deformation temperatures are displayed in Figure 2. The mechanical energy of the specimen is converted into heat energy during compression; therefore, the temperature rise of the sample is large at high strain rate, thus it is necessary to modify the experimental data of stress–strain curve for strain rate of 10 s^{-1} with temperature [19], and Figure 2(e) exhibits the modified curve. At fixed deformation temperature, both the flow stress and peak stress increased with strain rate, indicating the positive

Peer-reviewed version available at Materials 2020, 13, 3739; doi:10.3390/ma13173739

strain rate sensitivity of the alloy. At fixed strain rate, both the flow stress and peak stress declined with temperature, suggesting the heat-sensitive nature of the alloy [20].

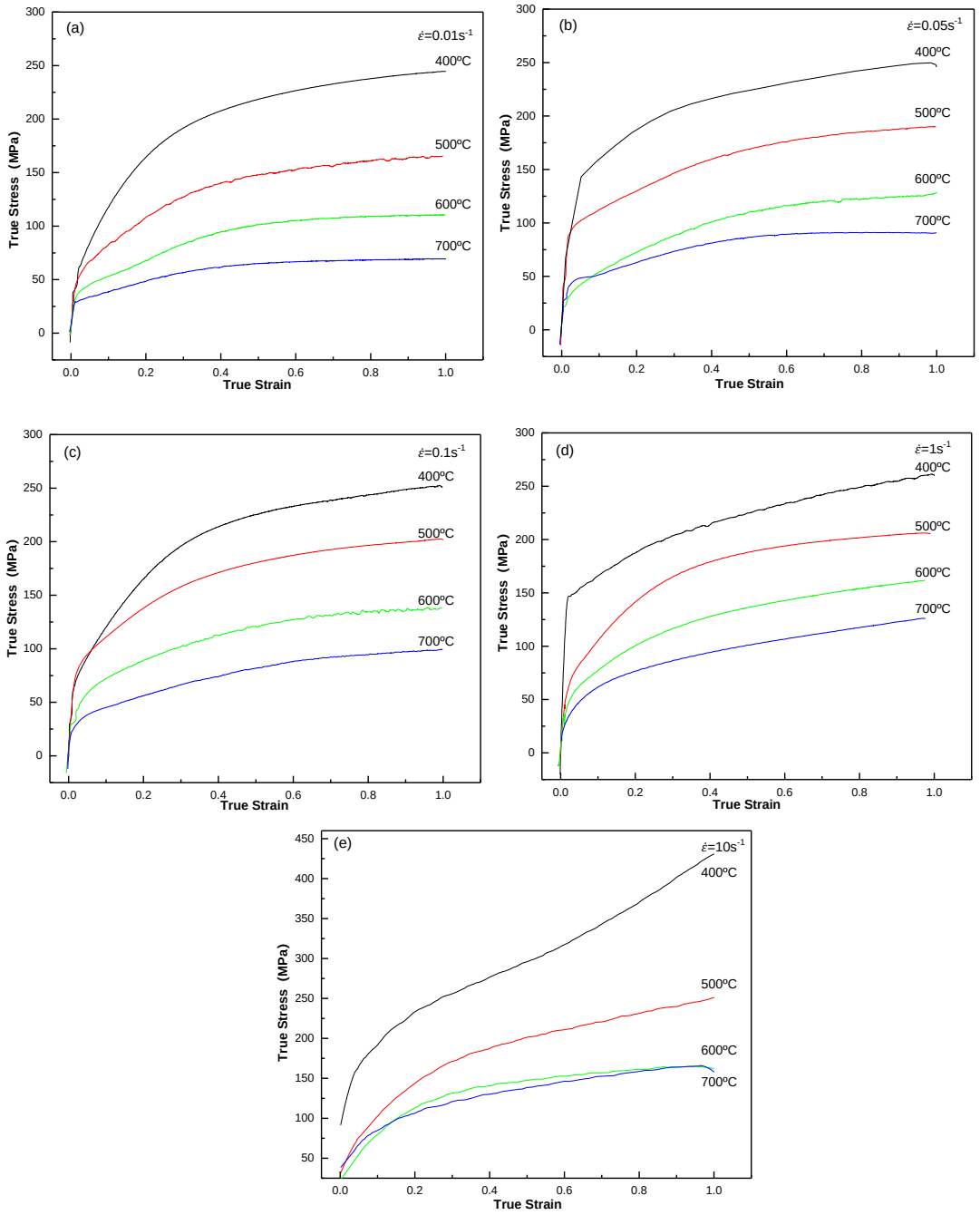

Figure 2. True stress–true strain behaviors of Cu–0.55Sn–0.08La alloy subjected to various strain rates at different temperatures: (a) $\dot{\varepsilon}$ = 0.01 s^{-1}, (b) $\dot{\varepsilon}$ = 0.05 s^{-1}, (c) $\dot{\varepsilon}$ = 0.1 s^{-1}, (d) $\dot{\varepsilon}$ = 1 s^{-1}, and (e) $\dot{\varepsilon}$ = 10 s^{-1}.

The shape of the flow curves exhibited the dependence on the initial grain size and steady DRX grain Size [21]. Compared to recrystallized grain size (0.06 mm) after dynamic compression (Figure 7), the initial grain size (1.40 mm) of the test sample was significantly large (Figure 3). As a result, no peak or only one peak appeared in the stress–strain curve.

Moreover, the shape of each flow curve strongly depended on the solution concentration [22].

The flow stress (peak value and steady flow stress) of the copper alloy was always higher than that of pure copper under the same deformation conditions of temperature and strain rate. The mass fractions of Sn and La in the specimens were determined to be 0.55 and 0.08%, respectively. Both the

Peer-reviewed version available at Materials 2020, 13, 3739; doi:10.3390/ma13173739

Cu-La intermetallic compounds and Sn solute elements increased the dislocation movement difficulty in the copper matrix, thereby increasing the flow stress of the copper alloy.

At the strain rates of 0.01–1 s^{-1} and 400 °C, the flow stress first increased rapidly with strain and then tended to increase slowly, showing typical work hardening features. At strain rates of 10 s^{-1}, the flow stress increased faster than the low strain rate due to the obvious work hardening effect. The final stage of the curve still displayed an upward trend, indicating the dominance of the work hardening effect. With the increase in the strain rate, the peak value of flow stress increased slowly from 0.01 to 1 s^{-1}. For strain rates exceeding the critical value (1 s^{-1}) the peak value of flow stress increased significantly. When the strain rate is rapid, the plastic deformation occurs in a short time, the deformed grains cannot recover or recrystallize in time, the work hardening effect is significant, the dislocation density in the alloy increases, and the flow stress peak value increases significantly.

At 500–600 °C, the flow stress first increased rapidly with strain and then tended to stabilize without obvious flow stress peaks and sharp softening trend. With the increase of strain rate from 0.01 to 0.05 s^{-1} at 500 °C, the peak value of flow stress increased rapidly and then tended to stabilize from 0.1 to 1 s^{-1}. At strain rates exceeding 1 s^{-1}, the peak value of the flow stress enhanced significantly. From 0.01 to 1 s^{-1} at 600 °C, the peak value of the flow stress further increased. As strain rate reached 1 s^{-1}, the peak value of flow stress increased slowly.

At 700 °C, the flow stress increased rapidly with strain and then tended to stabilize, indicating the important role of dynamic softening in the process. As strain rate incremented, the peak value of the flow stress increased gradually. At 0.01–0.05 s^{-1}, the flow stress tended to stabilize as strain increased. From 0.1 to 10 s^{-1}, the flow stress tended to increase slightly with further increase in strain.

Above all, during hot working, strain hardening and dynamic recovery occurred simultaneously at low temperature or high strain rate. With dislocation proliferation, accretion, recombination, and annihilation, the dislocation distribution was observed first to be uneven and then gradually evolved into an independent cellular structure in different dislocation tangled areas [21]. This led to formation of dislocation cells and reduction in dislocation density. Consequently, stress–strain curve increased slowly at 400 °C (Figures 2(a) and 2(b)). At high deformation temperatures or low strain rates, the deformation process was accompanied by the formation and growth of recrystallized crystal nuclei, and softening rate of the alloy appeared greater than or equal to the deformation hardening rate [23]. Thus, the stress–strain curve tended to stabilize (Figures 2(a) and 2(b) at 700 °C). At deformation hardening rate equivalent to dynamic recovery and dynamic recrystallization rate, the stress–strain curve was stable (Figures 2(a) and 2(b) at 600 °C). The reason for the above mentioned different laws can be attributed to the competition between dynamic hardening and dynamic softening phenomena.

On the other hand, since the alloy was characterized with low stacking fault energy, its extended dislocations were very wide. Moreover, the dislocations were difficult to extricate from the dislocation network, as well as challenging to offset each other through cross slip and climb. At the beginning of deformation, the recovery of the sub-structure was very slow. This led to very high dislocation density in the sub-structure, a very small structure of the sub crystal, and many dislocation tangles in the cell wall.

3.2. Microstructure

Peer-reviewed version available at Materials 2020, 13, 3739; doi:10.3390/ma13173739

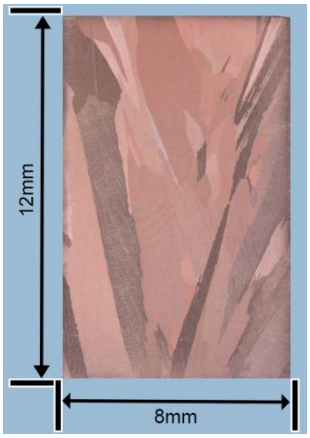

Figure 3. Macrostructure of uncompressed specimen.

The macrostructure of an uncompressed specimen is presented in Figure 3. The morphology was generated by different orientations of casting grains, where single-phase microstructure was etched into different colors. At the edge of the ingot, oblique columnar crystals were formed attributed to horizontal cooling direction and upward vertical movement. The cooling rate of the ingot center decreased and a few grains with smaller sized appeared. The average length of the grains on the right side was estimated to be about 3 mm and width was around 0.5 mm. The average length of the grains on the left side was about 10 mm and width was around 1 mm. Furthermore, the grains on the left and right sides showed obvious boundaries. This is due to the different cooling rates on both sides of the ingot.

The microstructures of the alloy deformed at 400 °C under different strain rates are illustrated in Figure 4. Owing to the large initial grain size, macro coordinated deformation is difficult. The deformation of each grain appeared to be extremely uneven. Moreover, many slip bands and adiabatic shear bands were present in some grains [24], which were terminated at the grain boundary [25,26]. Under compression deformation, the grains rotated to become gradually perpendicular to the compression direction. Compared to Figure 6(a), the slip bands in the grains became denser in Figure 6(b) as strain rate increased.

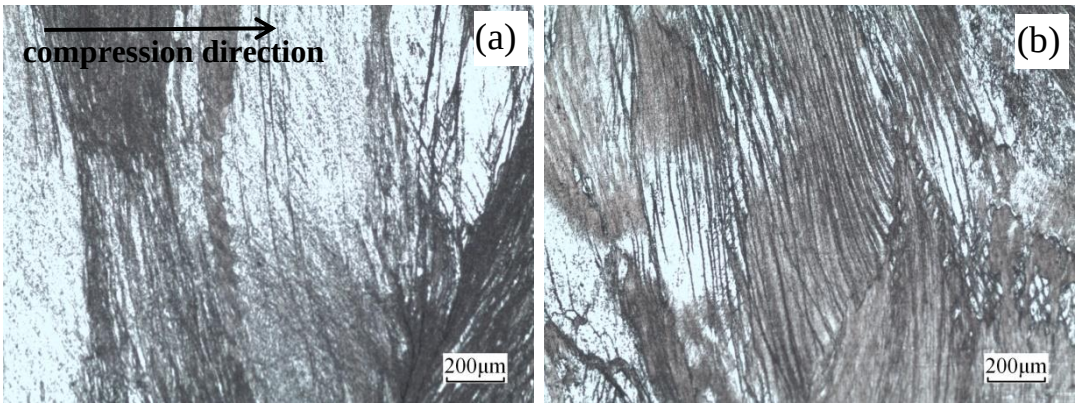

Figure 4. Microstructures of the alloy deformed at 400 °C and different rates: (a) $\dot{\varepsilon} = 0.01\ s^{-1}$ and (b) $\dot{\varepsilon} = 10\ s^{-1}$.

The microstructures of the alloy deformed at 500 °C and different strain rates are presented in Figure 5. At low strain rate ($\dot{\varepsilon} = 0.01\ s^{-1}$), shear bands still existed and dynamically recrystallized grains were found in the shear bands (Figure 5(a)). Thus, the dynamic recrystallization occurred locally with formation of large numbers of fine dynamic recrystallized grains at the grain boundary. This led to formation of large numbers of "necklace structures". As strain rate increased, at higher strain rate ($\dot{\varepsilon} = 10\ s^{-1}$), numerous fine recrystallized grains and annealing twin appeared (Figure 5(b)). The wave-like grain boundaries are usually observed in Figure 5(b) under DRX conditions.

Peer-reviewed version available at Materials 2020, 13, 3739; doi:10.3390/ma13173739

Noteworthy, Figure 5(b) exhibits that annealing twins are evolved in dynamic grains, although their density is lower than that for statically annealed grains.

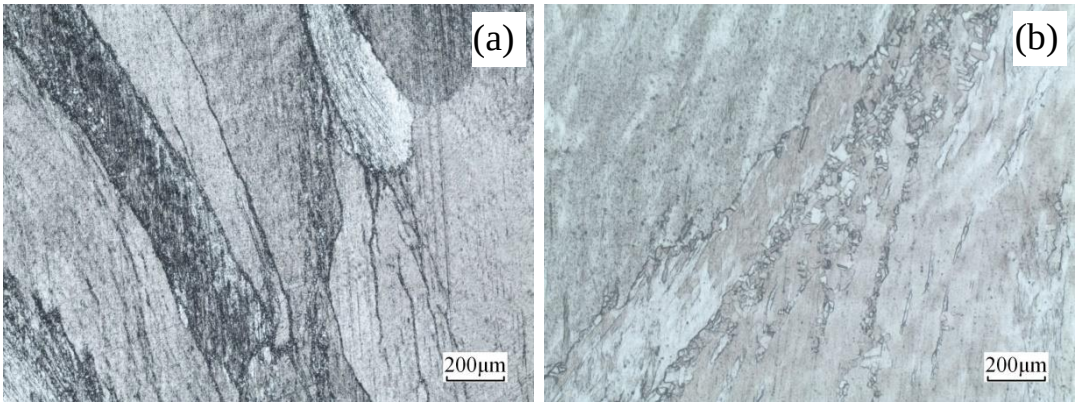

Figure 5. Microstructures of the alloy deformed at 500 °C and different rates: (a) $\dot{\varepsilon}$ = 0.01 s^{-1} and (b) $\dot{\varepsilon}$ = 10 s^{-1}.

The microstructures of the alloy deformed at 600 °C and different strain rates are provided in Figure 6. At low and high strain rates ($\dot{\varepsilon}$ = 0.01 s^{-1} and $\dot{\varepsilon}$ = 10 s^{-1}), dynamically recrystallized grains were noticed and became obvious as strain rate increased (Figure 6(b)). Besides, the grain boundary preferentially nucleated (Figure 6), and dynamically recrystallized grains gradually expanded and grew around by devouring the surrounding deformed matrix. The latter was due to the grain boundary, which possessed basic conditions of recrystallization nucleation of large-angle interface with high-density defects and superior deformation energy. At this place, recrystallization exhibited priority for nucleation and growth, forming fine and equiaxed recrystallization structure.

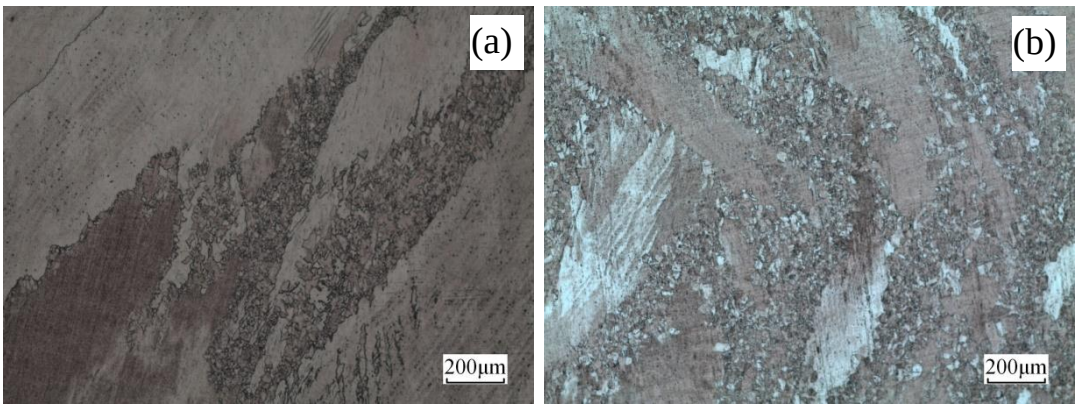

Figure 6. Microstructures of the alloy deformed at 600 °C and different rates: (a) $\dot{\varepsilon}$ = 0.01 s^{-1} and (b) $\dot{\varepsilon}$ = 10 s^{-1}.

The microstructures of the alloy deformed at 700 °C at different strain rates are displayed in Figure 7. Fine recrystallization in the center of Figure 7(b) is observed, and the boundary between recrystallized grain and initial grain appears to be clear. During dynamic recrystallization, the La rich phase prevented the grain boundary from migrating, thereby reducing the size of the dynamic recrystallization grain.

On the other hand, the recrystallized grain sizes at high strain rates were larger at the same temperature since higher deformation temperatures led to slower deformation rates. Furthermore, more complete thermal activation processes led to less storage energy after deformation, thus delaying recrystallization and forming smaller recrystallized grain size at low strain rates [27].

Peer-reviewed version available at Materials 2020, 13, 3739; doi:10.3390/ma13173739

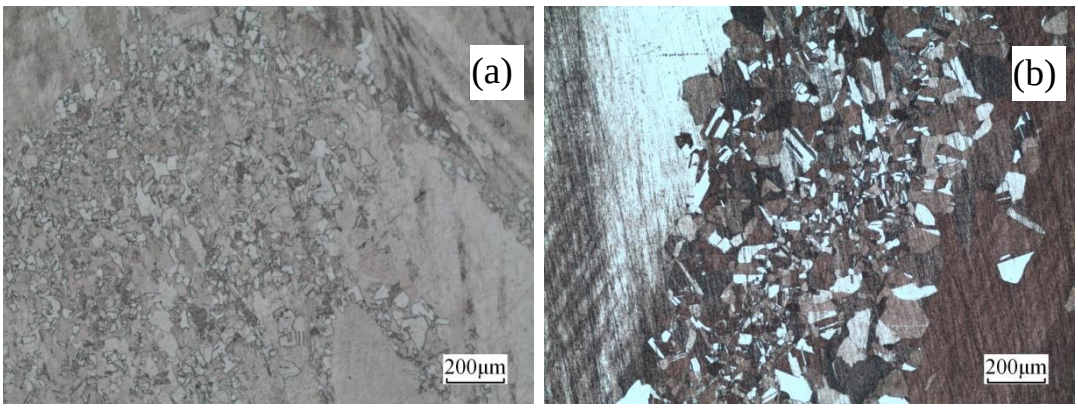

Figure 7. *Microstructures of the alloy deformed at 700 ℃ and different rates: (a)* $\dot{\varepsilon}$ *= 0.05 s*$^{-1}$ *and (b)* $\dot{\varepsilon}$ *=10 s*$^{-1}$.

3.3. Constitutive equations

Constitutive equations are often used in hot working conditions to calculate forces during processing at certain setting rates. The modeling of the processing stage must take into account the non-uniform distribution of strain, strain rate, and temperature, as well as their variations with time. The model may need several constitutive functions depending on the complexity of the flow curves [28]. The constitutive relationship describing the flow stress behavior during hot deformation can be expressed by the Arrhenius equation. This type of constitutive relation is justified when strain hardening can be ignored. At 400 °C, the strain hardening effect is significant, in particular, in the case of high strain rate (10 s^{-1}). At 500–600 ℃, the strain hardening effect is slight. Therefore, the calculation process of the constitutive equation was mainly carried out at 500, 600, and 700 °C.

The corresponding temperature and strain rate dependence of plastic deformation can be analyzed by using the Zener–Holloman parameter (Z), also known as temperature compensated strain rate (especially applicable for high-temperature deformation). The respective constitutive equation can be expressed according to Eq. (1) [29] as follows:

$$Z = A \cdot [\sinh(\alpha\sigma)]^n = \dot{\varepsilon} \cdot \exp(Q/RT) \quad (1)$$

where A, α, and n are the temperature-independent material constants, R is the universal gas constant (8.314 J mol^{-1} K^{-1}), T is temperature (K), Q is the apparent activation energy of deformation (J mol^{-1}), $\dot{\varepsilon}$ is strain rate (s^{-1}), and σ is true stress (MPa).

In the constitutive analysis, the effects of temperature and strain rate on flow stress can be adequately expressed according to Eq. (2) [30]:

$$\dot{\varepsilon} = A \cdot [\sinh(\alpha\sigma)]^n \cdot \exp(-Q/RT) \quad (2)$$

Notably, Eq. (2) can be expressed in three different formats depending on the stress levels: power function for low stress (Eq. (3)), exponential function for high stress (Eq. (4)) [31], and hyperbolic sine function for any given stress (Eq. (2)).

$$\dot{\varepsilon} = A_1 \cdot \sigma^{n_1} \cdot \exp\left(-\frac{Q}{RT}\right) \qquad \alpha\sigma < 0.8 \quad (3)$$

$$\dot{\varepsilon} = A_2 \cdot \exp(\beta\sigma) \cdot \exp\left(-\frac{Q}{RT}\right) \qquad \alpha\sigma > 1.2 \quad (4)$$

where A1 and A2 are material constants, and n1 and β are related to strain rate sensitivity index.

Eqs. (2)–(4) can be written as:

Peer-reviewed version available at Materials 2020, 13, 3739; doi:10.3390/ma13173739

$$\ln\dot{\varepsilon} = n\ln[\sinh(\alpha\sigma)] + \ln A - \left(\frac{Q}{RT}\right) \quad (5)$$

$$\ln\dot{\varepsilon} = n_1\ln\sigma + \ln A_1 - \left(\frac{Q}{RT}\right) \qquad \alpha\sigma < 0.8 \quad (6)$$

$$\ln\dot{\varepsilon} = \beta\sigma + \ln A_2 - \left(\frac{Q}{RT}\right) \qquad \alpha\sigma > 1.2 \quad (7)$$

The parameters n_1, β, and n were calculated by plotting $\ln\dot{\varepsilon}$ versus $\ln\sigma$ (Figure 8(a)), $\ln\dot{\varepsilon}$ versus σ (Figure 8(b)), and $\ln\dot{\varepsilon}$ versus $\ln[\sinh(\alpha\sigma)]$ (Figure 8(c)), respectively. The material constant n_1 was estimated by the average of the three slopes of the linear fits of $\ln\dot{\varepsilon}$ versus $\ln\sigma$ with lower peak stress. β was determined by the average of the three slopes of the linear fits of $\ln\dot{\varepsilon}$ versus σ with higher peak stress and $\alpha = \beta/n_1$. The constant n presented the slope of the linear fit of $\ln\dot{\varepsilon}$ versus $\ln[\sinh(\alpha\sigma)]$. Accordingly, the value of n_1 was estimated to be 13.7935, β was 0.0898, α was 0.00651, and n was 10.2378.

The apparent activation energy Q for the plastic deformation can be expressed in terms of Eq. (8):

$$Q = 1000 \cdot R \cdot \left[\frac{\partial\ln\dot{\varepsilon}}{\partial\ln[\sinh(\alpha\sigma)]}\right]_T \cdot \left[\frac{\partial\ln[\sinh(\alpha\sigma)]}{\partial\left(\frac{1000}{T}\right)}\right]_{\dot{\varepsilon}} = 1000nRK \quad (8)$$

where $K = \left[\frac{\partial\ln[\sinh(\alpha\sigma)]}{\partial\left(\frac{1000}{T}\right)}\right]_{\dot{\varepsilon}}$ is the slope of linear fit in Figure 8(d).

Accordingly, the value of K was calculated as 3.073796 and Q was 261.649 kJ mol^{-1}. On the other hand, the activation energy of thermal deformation of pure copper with different impurity contents is around 208–245 kJ mol^{-1} [22,32]. Moreover, higher impurity contents should yield greater activation energies of thermal deformation. The activation energy of thermal deformation of Cu-0.55Sn-0.08La alloy was estimated to be 261.649 kJ mol^{-1}, indicating that the addition of Sn and La to the copper matrix increased the flow stress of the alloy. This result may be attributed to the interaction between solute atoms Sn and dislocations and grain boundaries, which hindered the dislocation sliding, climbing, and grain boundary migration. These features were unfavorable to the nucleation and growth of recrystallization, thereby limiting the recrystallization process. On the other hand, rare earth La and impurity atoms in liquid copper formed high melting point compounds, which dispersed on the grain boundary. During compression deformation, the dispersed phase was pinned at the grain boundary of the copper alloy, thus hindering the migration of grain boundary. Moreover, the activation energy of Cu-0.55sn-0.08la alloy was found to be higher than that of pure copper.

Peer-reviewed version available at Materials 2020, 13, 3739; doi:10.3390/ma13173739

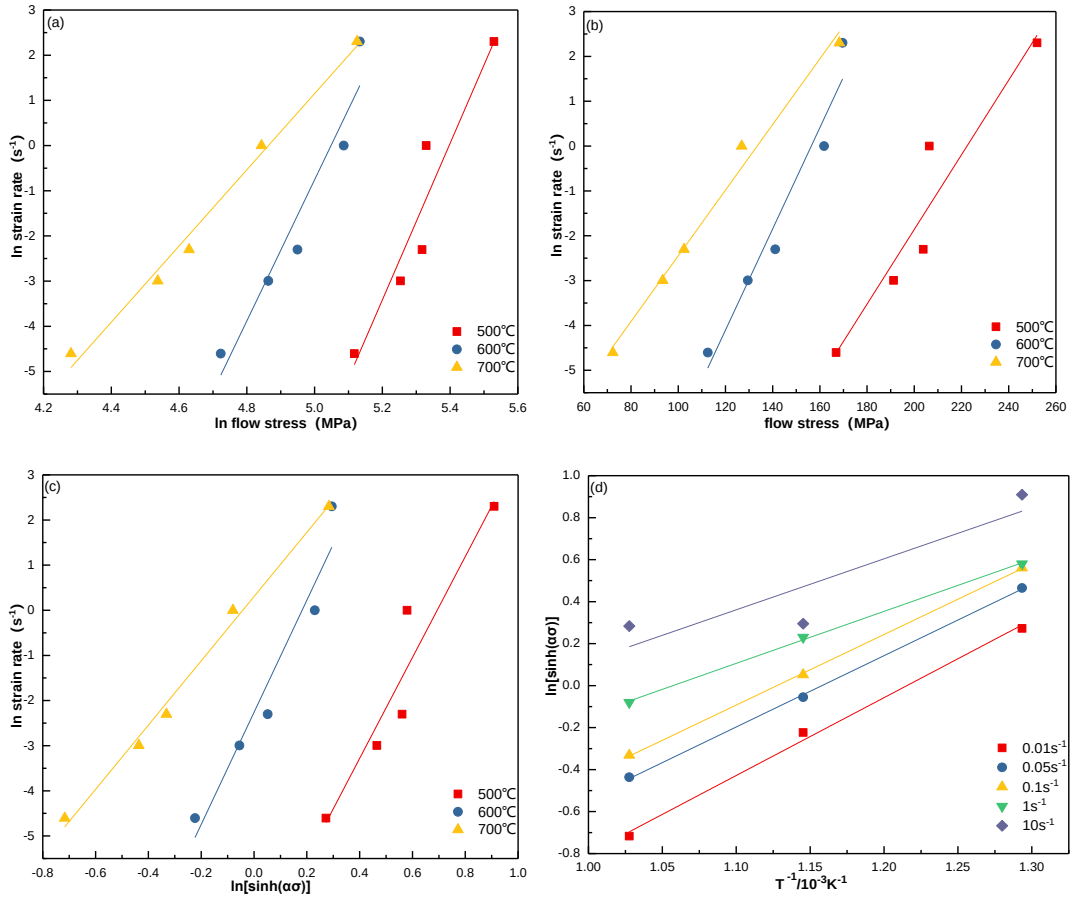

Figure 8. Variations of peak stress (σ) with strain rate (ε̇) and deformation temperature (T) of Cu−0.55Sn-0.08La alloy: (a) lnσ versus lnε̇, (b) σ versus lnε̇, (c) lnε̇ versus ln[sinh(ασ)], and (d) T−1 versus ln[sinh(ασ)].

To calculate n and ln A, ln[sinh(ασ)] was plotted as a function of lnZ and the results are provided in Figure 9. The value of n was estimated to be 9.76008 and ln A was 33.66562.

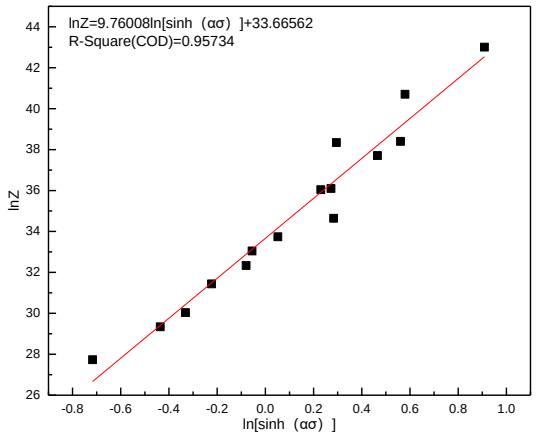

Figure 9. Plot of ln Z versus ln [sinh(ασ)] for evaluating ln A.

Based on the above mentioned analyses, the constitutive equation of Cu–0.55Sn–0.08La at high temperatures was determined as: $\dot{\varepsilon} = A \cdot [\sinh(\alpha\sigma)]^n \cdot \exp\left(-\frac{Q}{RT}\right)$.

As a result, Eq. (9) can be deduced as:

Peer-reviewed version available at Materials 2020, 13, 3739; doi:10.3390/ma13173739

$$\dot{\varepsilon} = [\sinh(0.00651\sigma)]^{10.2378} \cdot \exp\,(33.6656 - 261.649/\mathrm{RT}) \quad (9)$$

4. Conclusions

Hot deformation of Cu-0.55Sn-0.08La (wt.%) alloy was successfully studied using gleeble-3180 testing machine at deformation temperatures (400–700 °C) and various strain rates. The following conclusions were drawn:

1. The flow stress of Cu-0.55Sn-0.08La alloy decreased with deformation temperature and increased with strain rate. At low temperature (400 °C) or high strain rates (1 and 10 s^{-1}), the stress–strain curve increased with deformation. At high deformation temperature (700 °C) or low strain rates (0.01 and 0.05 s^{-1}), the deformation process was accompanied by formation and growth of recrystallized nuclei. Besides, the softening rate of the alloy was equal to the deformation hardening rate, and stress–strain curve tended to stabilize.

2. At 500–700 °C and 0.01–10 s^{-1}, the relationship between peak flow stress of Cu-0.55Sn-0.08La alloy and strain rate was determined as : $\dot{\varepsilon} = A \cdot [\sinh(\alpha\sigma)]^n \cdot \exp(-Q/RT)$ and thermal activation energy Q was 261.649 kJ mol^{-1}. Thus, the constitutive equation can be expressed as: $\dot{\varepsilon} = [sinh(0.00651\sigma)]^{10.2378} \cdot \exp\left(33.6656 - \frac{261.649}{RT}\right)$.

3. The microstructure of Cu-0.55Sn-0.08La alloy showed the presence of slip bands and shear bands in the grains at deformation temperature of 400 °C. Recrystallization grains were noticed near the shear band at the grain boundary as deformation temperature increased. At 700 °C, the dynamic recrystallization appeared to be relatively complete with the growth of recrystallization grains.

Author Contributions: Conceptualization, H.S.; methodology, H.S.; software, H.S.; validation, H.S.; formal analysis, H.S.; investigation, H.S. and Y.L.; resources, H.S. and Z.P.; data curation, H.S.; writing—original draft preparation, H.S.; writing—review and editing, H.S., Z.P., and L.Z.; visualization, H.S.; supervision, H.S.; project administration, H.S.; funding acquisition, H.S. All authors have read and agreed to the published version of the manuscript.

Funding:

(1) This research was funded by the research and development of high speed current collection system for rail transit, grant number RD28.

(2) The Priority Academic Program Development of Jiangsu Higher Education Institutions, China.

Conflicts of Interest: The authors declare no conflict of interest.

References

1. [1] Wu,P.Y. ; Xie,S.S.; Huang,G.J. Materials and Process Technics of Copper Contact Wires for High-Speed Train. CHINESE JOURNAL OF RARE METALS **2006**,30,202-208.
2. [2] Zhang,Yi. ;Xu,Q.Q. ;Chai,Z. ; etc. High temperature deformation behavior and deformation mechanism of Cu-Cr-Zr-Ag alloy. The Chinese Journal of Nonferrous Metals **2015**,25, 931-937.
3. [3]Zhang,H.G. ;Zhang ,H. ;Liu ,W.R. ;etc. Rheologic Stress of C194 Copper Alloy Under Hot Compression Deformation. Natural Science Journal of Xiangtan University**2003**,25,82-86.
4. [4]Yao, S. ;Liu,P. ; Liu, X.K. ;etc. Hot Plastic Deformation Behavior of KFC Copper Alloy. SHANGHAI NONFERROUS METALS **2013**,34,15-19.
5. [5]Liu, P.; Fan,L. ;Jia,S.G.; etc. Study on dynamic recrystallization behavior and microstructure evolution of Cu-Ni-Si-Cr alloy. J.University of Shanghai for Science and Technology**2009**, 31,548-550.
6. [6] Zhang,Y. ; Liu, P. ; Tian, B.H. ;etc. Hot deformation behavior and processing map of Cu-Ni-Si-P alloy. Trans. Nonferrous Met. Soc. China **2013**,23 ,2341−2347.
7. [7] Wang, M.H.; Yang,Y.C. ; Tu,S.L. ;etc. A modified constitutive model and hot compression instability behavior of Cu−Ag alloy. Trans. Nonferrous Met. Soc. China **2019**,29,764-774.

Peer-reviewed version available at Materials 2020, 13, 3739; doi:10.3390/ma13173739

8. [8] Shen,K.; Wang, M.P.; Guo,M.X.;etc. Study on High Temperature Deformation Characteristics of Cu-0.23%$A1_2O_3$ Dispersion-strengthened Copper Alloy.ACTA METALLURGICA SINICA **2009**, 45, 597-604.
9. [9] Zhang,Y. ; Chai,Z. ; Xu,Q.Q. ; etc. Hot deformation behavior and processing maps of Cu-0.8Cr-0.3Zr alloy. TRANSACTIONS OF MATERIALS AND HEAT TREATMENT **2015**,36,7-12.
10. [10] Zhang,Y. ; Xu,Q.Q. ; Chai,Z. ;etc.. High temperature deformation behavior and deformation mechanism of Cu-Cr-Zr-Ag alloy. The Chinese Journal of Nonferrous Metals **2015**,25 ,931-937.
11. [11] Tian,K.; Tian,B.H. ; Liu,Y. ;etc. Hot Deformation Behavior of Cu-1.0%Zr-0.15%Y Alloy with High Zr Content. RARE METAL MATERIALS AND ENGINEERING **2018**,47,1143-1148.
12. [12] Xu, Q.Q. ; Zhang,Y.; Chai,Z. ; etc. High temperature deformation behavior and microstructure evolution of Cu-Cr-Zr-Nd alloy.The Chinese Journal of Nonferrous Metals **2015**,25,668-673.
13. [13] Li,R.Q. ; Tian ,B.H. ; Zhang,Y. ; etc. Hot deformation behavior of Cu-Cr-Zr-Ce alloy at elevated temperature. Jorunal of Functional Materials **2013**,44, 2036-2046.
14. [14] Wang,B.J. ;Tian,B.H. ;Zhang,Y. ;etc. Hot deformation behavior and processing maps of Cu-0.8%Mg-0.2%Fe alloy.Transactions of Materials and Heat Treatment **2018**,39,145-151.
15. [15] Sun ,G.Q. ;Liu,Y. ;Tian,B.H. ;etc. Hot deformation behavior and mechanism of Cu-0.8Mg alloy.Transactions of Materials and Heat Treatment **2018**,39,135-142.
16. [16] Z. Gronostajski. The deformation processing map for control of microstructure in CuAl9.2Fe3 aluminium bronze.Journal of Materials Processing Technology **2002**,125,119-124.
17. [17] Yang,C.X. ; Chen,Z.P. ;Li ,H.Q. ; etc. Flow Stress Feature of Aiuminium Bronze Alloy under Hot Deformation. RARE METAL MATERIALS AND ENGINEERING **2010**,39,126-129.
18. [18] Li ,Y. ;Liu ,Y. ; Tian ,B.H. ;etc. Hot Compression Deformation Behavior and Processing Map of Cu-0.4Zr-0.15Ce Alloy. JOURNAL OF THE CHINESE SOCIETY OF RARE EARTHS **2016**,34,221-228.
19. [19]Chen S.C.,He S.X., Wu B.J.,;etc. THE COLLATING AND CORRECTING OF DATA IN HOT COMPRESS ING TEST FOR GLEEBLE MATERIAL HOT MODELING TEST MACHIN E. Journal of Tangshan Institute of Technology**1993**,4,40-48.
20. [20]Li, R.Q. ; Tian, B.H. ; Zhang, Y. ;etc. Effects of Y addition on hot deformation behavior of Cu-Cr-Zr alloy at elevated temperature. TRANSACTIONS OF MATERIALS AND HEAT TREATMENT **2014**,35,51-56.
21. [21] Taku Sakai. DYNAMIC RECRYSTALLIZATION MICROSTRUCTURES UNDER HOT WORKING CONDITIONS. Journal of Materials Processing Technology **1995**,53, 349-361.
22. [22] Gao, W. ; Belyakov, A. ;Miura, H. ;etc. Dynamic recrystallization of copper polycrystals with different purities. Materials Science and Engineering A**1999**, 265, 233–239.
23. [23] N. Srinivasan; Y.V.R.K. Prasad; P. Rama Rao. Hot deformation behaviour of Mg-3Al alloy—A study using processing map. Materials Science and Engineering A **2008**(476),146–156.
24. [24] Li, J.W.; Li, M.Y.; Guo, X.L.;etc. FORMATION OF ADIABATIC SHEAR BANDS IN THE FATIGUED COPPER SINGLE CRYSTAL DEFORMED AT HIGH STRAIN RATE.ACTA METALLURGICA SINICA **2005**,41,161-166.
25. [25] Li,J.W.; Lin, D.C. Metallographic Atlas of metal materials,1rd ed.; Mechanical Industry Press: Beijing,China,**2006**;p.1523.
26. [26] Humphreys F.J., Hatherly M.RECRYSTALLIZATION AND RELATED ANNEALING PHENOMENA, 2rd ed.; :Elsevier: Amsterdam, Netherlands,**2004**;p.240.

Peer-reviewed version available at Materials 2020, 13, 3739; doi:10.3390/ma13173739

27. [27] Yu Y.N., Yang P., Qiang W.J.,;etc. Fundamentals of Materials Science, 1rd ed.; Higher Education Press: Beijing,China, **2006**;p.736.
28. [28]McQueen, H.J.; Ryan, N.D. Constitutive analysis in hot working. Materials Science and Engineering A**2002**,322,43-63.
29. [29]Madan, P. ; Ari,S. ;Mahesh,C.;etc. Constitutive modelling of hot deformation behaviour of a CoCrFeMnNi high-entropy alloy. Science and Technology of Advanced Materials **2020**,21, 43-55.
30. [30] Zhang, L. ; Li, Z.; Lei, Q. ;etc. Hot deformation behavior of Cu–8.0Ni-1.8Si-0.15Mg alloy. Materials Science and Engineering A **2011**,528,1641–1647.
31. [31] RYAN, N.D. ; McQUEEN, H.J.; Dynamic Recovery and Strain Hardening in the Hot Deformation of Type 317 Stainless Steel. Materials Science and Engineering **1986**,81,259-272.
32. [32] Zhao, R.L.; Liu, Y.; Tian, B.H.; etc. High temperature deformation behavior of pure copper.HEAT TREATMENT OF METALS **2011**,36,17-20.